Revision 2

Kinetics of deuteration in andradite

Peipei Zhang[1,2], Jannick Ingrin[2]*, Christophe Depecker[2] and Qunke Xia[1]

[1] School of Earth and Space Sciences, University of Science and Technology of China, Hefei 230026, China

[2] Unité Matériaux Et Transformations, CNRS UMR 8207, Université Lille1, Bâtiment C6, 59655 Villeneuve d'Ascq, France

*E-mail: jannick.ingrin@univ-lille1.fr

Abstract

The hydrogen mobility in andradite single crystals from an iron-skarn deposit was investigated through H-D and D-H exchange experiments. Thin slices were annealed in a horizontal furnace flushed with a gas mixture of $Ar/D_{2(10\%)}$ and $Ar/H_{2(10\%)}$ at ambient pressure between 400 °C and 700 °C. FTIR analyses were performed before and after each annealing run. Between 15% and 35% of the original OH content remained in the crystal structure at the end of the deuteration experiments. This contrasts with the results of similar experiments performed in other NAMs, where all hydrogen atoms are replaced by deuterium in the structure. However, because a steady state was reached at the end of the experiments, the diffusion law for the exchange process was determined as: $D_{H\text{-}D} = D_0 \exp[-(96 \pm 11)\ kJ/mol/RT]$, with $\log D_0 = -5.9 \pm 0.7$ (in m^2/s). The activation energy is

similar to that for hydrogen diffusion in grossular, but H diffusivity is more than 2 orders magnitude faster. Our results demonstrate that, because major element composition has a major effect on H-D diffusion laws, it must be considered in any discussion of δD signatures in garnets. In andradite-rich garnets, hydrogen isotope data can only be used to record short, low-grade metamorphic or metasomatic events, at temperatures lower than 400 °C.

Keywords: hydrogen, andradite, FTIR, diffusion, deuterium, garnet.

Introduction

Hydrogen species in nominally anhydrous minerals (NAMs), which occurs as a minor or trace constituent in the crystal structure, have received growing interest during the past decades because of its disproportionately large effect on the physical and chemical properties of minerals/rocks (Rossman and Aines 1991; Bell and Rosssman 1992a, 1992b; Thompson 1992; Ingrin and Skogby 2000). The hydrogen content may be used to identify the nature of fluids being present during metamorphic and metasomatism events and to trace the origin of these fluids (Matveev et al. 2001; Xia et al. 2005; Sheng et al. 2007; Chen et al. 2011). Knowledge of hydrogen diffusivity is essential to determine the origin of hydrogen during metamorphic and metasomatic events.

Large amounts of hydrogen can be incorporated as OH in both natural and synthetic andradite (Kobayashi and Shoji 1987; Armbruster and Geiger 1993; Armbruster 1995). High OH contents have also been reported for Fe^{3+}-rich garnets such as melanite and schorlomite (Lager et al. 1989; Locock et al. 1995). Armbruster and Geiger (1993) proposed that incorporation of OH into Ca-Fe garnet can reduce the internal strain in the structure of Ca-Fe^{3+} garnets. The hydrogarnet substitution [$(O_4H_4)^{4-}$ = $(SiO_4)^{4-}$], which was first established for hydrogrossular (Cohen-Addad et al. 1967; Lager et al. 1987, 1989), was also confirmed in andradite (Armbruster 1995), although other kinds of OH defects may also occur in that mineral (Cho and Rossman 1993).

Few studies on the diffusion of hydrogen in garnets have been published (pyrope: Wang et al. 1996; Blanchard and Ingrin 2004a,b; grossular: Kurka et al. 2005; andradite: Kurka 2005; Ingrin and Blanchard 2006; Phichaikamjorn et al. 2012). These studies have shown that the activation energies of the extraction laws are much higher than in most ferromagnesian silicates; they range between 200 and 350 kJ/mol and the diffusion coefficients cover two orders of magnitude in the temperature range of 700–1050 °C. It has been shown that it is difficult to model the evolution of H concentration of garnets with time by a simple diffusion process (Kurka 2005; Phichaikamjorn et al. 2012). This is particularly true for andradite garnets where it was frequently observed that 10 to 20 % of the original H content remained in the crystal after annealing (Kurka 2005;

Phichaikamjornwut et al. 2012). Several explanations were proposed for this behavior but no definitive solution was found. Furthermore, the mechanisms involved in H extraction in garnets remain largely unknown. Although, the redox-reaction $Fe^{2+} + OH^- = Fe^{3+} + O^{2-} + 1/2H_2$ seems to be a possible candidate for pyrope and grossular (Blanchard and Ingrin 2004b, Forneris and Skogby 2004; Kurka 2005; Kurka et al. 2005), this process is not available for H extraction in andradites, which dominantly contain Fe^{3+} (Phichaikamjornwut et al. 2012).

Andradite is a rock-forming garnet typically found in skarns, which are often mined as ore deposits and found in contact metamorphic assemblages, like serpentinite. The hydrogen isotope information collected from andradite, if preserved during cooling, can be used to indicate the origin of H_2O in the fluids in contact with the crystals. Despite this, complete H-D exchange studies have only been performed using Dora Maira pyrope and grossular garnets (Blanchard and Ingrin 2004a; Kurka et al. 2005). The aim of this study was therefore to determine hydrogen mobility in andradite from H-D exchange experiments. Understanding H mobility in andradite will provide useful, complementary information to help identify the mechanisms of H exchange in this type of garnet and the data will be used to elucidate the role of H mobility in the extraction/incorporation kinetics in andradite. The knowledge of H mobility laws in andradite provides a

quantitative framework for the interpretation of data on natural andradites and their use to identify the nature of fluids-rock interactions.

Experimental methods

Sample description and preparation

The andradite samples used in this study come from an iron-skarn deposit on Serifos island, Greece and were collected by Andreas Kurka. The crystals are found in large geodes inside an almost monomineralic hedenbergite rock, which lies adjacent to a marble layer. The andradites form idiomorphic crystals of up to 5 cm in diameter and show a prominent zonation with a dark colored rim about 1 mm thick. In this study, eight thin slices from the core of two andradite crystals were cut and then polished on both sides using SIC paper of an increasingly fine grade and 1 μm alumina powder. The polished platelets, exhibiting a brownish-yellow color, are 140 to 671 μm thick and 2.0 to 5.0 mm in size. The thickness of platelets was measured with a Mitutoyo digital micrometer (± 3μm).

EMPA and LA-ICP-MS analysis

Andradite crystals used as starting material for diffusion experiments were analyzed with a Camera SX50 electron microprobe at the GET laboratory of the University of Toulouse with operating conditions set to an accelerating voltage of 15 kV and a beam

current of 20 nA. More than one hundred analytical points were recorded on 5 different slices. Major and trace element concentrations in the samples were measured using the LA-ICP-MS at the laboratory of the University of Science and Technology of China. Two sample slices were ablated in-situ using a Coherent company GeoLas pro ArF laser system operating with a beam wavelength of 193 nm at 10Hz and 10J/cm^2 energy per pulse. The signal intensity for each element was calibrated against a NIST 610 silicate glass. The Si^{29} content of samples, as determined by electron microprobe was used as an internal standard. The average compositions are presented in Table 1; uncertainties correspond to standard deviation of data dispersion. The chemical formula deduced from these measurements is assumed to be $(Ca_{2.992}Mn_{0.006}Mg_{0.001})(Fe)_{1.992}[Si_{2.981}(4H)_{0.025}]O_{12}$; where H contribution is deduced from FTIR measurements (see "Infrared analysis" below)

Annealing procedure

Stepwise annealing experiments were carried out at ambient pressure. Eleven experiments were performed at temperatures ranging from 400 to 700˚C (Table 2). We used a horizontal furnace with a lanthanium chromite heating element surrounding an alumina tube of 18 mm internal diameter within which the sample was placed. Experimental temperature, which had an estimated uncertainty less than ± 5 K, was controlled by a Pt/Pt-$Rh_{10\%}$ thermocouple that was located 3 mm away from the sample.

To conduct the H-D (H replacing D) and D-H (D replacing H) exchange experiments, the furnace was continuously flushed with a gas mixture of $Ar_{(90\%)}/D_{2(10\%)}$ flowing through deuterated water (99.9% D_2O, Sigma-Aldrich) and with a gas mixture of $Ar_{(90\%)}/H_{2(10\%)}$ flowing through deionized water respectively. Prior to heating, the alumina tube was flushed with the gas mixture for 30 minutes to ensure that the tube was completely filled with the gas mixture. The controller of the heating device for the furnace was programmed to accurately reach the temperature plateau within 1 hour and without temperature overshoot.

Infrared analysis

The hydroxyl content of each slice was determined by transmission infrared spectroscopy before and after each annealing experiment. Unpolarized spectra were acquired at room temperature with a Perkin Elmer 1760X FTIR spectrometer equipped with a LN_2 cooled MCT detector, a KBr beamsplitter and a globar IR source. Each spectrum was recorded on the same point in the centre of the slice, with an aperture of 100 μm in diameter. For each analysis 32 scans were collected at a spectral resolution of 2 cm^{-1}.

The OH homogeneity of the slices was systematically checked through multiple analyses. Slices SER04, SER15, SER17 and SER18 were perfectly homogeneous but slices SER13, SER16 and SER19 display sectors with different concentrations. The most

130 extreme difference in OH contents occurs in SER16, in which one sector contains more
131 than twice the concentration compared to the other sector (see SER16-P3 and SER16-P6
132 in Table 3). For slices SER13, SER16 and SER19, only sectors greater than 500 μm in
133 size, and with almost constant concentration were selected for further measurements.

134 To calculate the concentrations of OH and OD species, spectra were integrated
135 between 3750 to 3150 cm^{-1} and 2700 to 2500 cm^{-1}, respectively. For the OH region, a
136 linear baseline was used (Fig. 1a); 2). For the OD region, the spectrum of the sample at *t*
137 = 0 was systematically subtracted (Fig. 1b). The absorbance bands located at 2466 cm^{-1}
138 and 2640 cm^{-1} are related to internal vibrations of the crystal structure. The intensities of
139 these two bands remained constant throughout the annealing experiments.

140 Uncertainties in the calculated absorbance intensities were estimated from the
141 reproducibility of the analysis on the same slice and variation of the integral absorbance
142 due to a change of the position of the points used to anchor the baseline corrections.
143 Depending on the slice, the contribution of these errors to the measured integral
144 absorbance corresponds to less than 3% to 5% of the maximum value of absorbance of
145 OH (resp. OD). It is these extreme values that we chose to report in the plots of integral
146 absorbances. Errors associated with thickness measurements vary from 0.5% to 2%,
147 depending on the slice. This error has a minimal effect on the estimated water contents

and no effect on the calculated diffusion coefficients since the thickness of the slices is kept constant during annealing experiments.

The use of a single absorption coefficient to calculate the water content of garnets is still under discussion due to the complexity of the spectra (Maldener et al. 2003). Water concentrations of 0.18 (± 0.05) and 0.067 (± 0.013) wt% H_2O are obtained using the calibration for grossular (Rossman and Aines 1991), and the wavenumber-dependent calibration of Libowitzky and Rossman (1997), respectively. The absorption coefficient proposed by Maldener et al. (2003) leads to a value of 0.30 (± 0.23) wt% H_2O. We note that uncertainty in the calculated water contents is high because no reliable specific calibration for andradite has yet been proposed. Even if, the suitability of the general calibration of Libowitzky and Rossman (1997) to quantify OH content in garnet has been questioned (Maldener et al. 2003), we chose here to use the average of the three values (0.18 ± 0.12) to estimate the water concentration in our samples. In this study, uncertainties about absolute OH contents do not affect the diffusion results because these are only dependent on the relative decrease or increase of OH and OD band intensities after annealing.

Analytical solution

It was assumed that the integral absorbance of OH and OD regions are linearly proportional to the respective concentrations of each species in the garnet. Since the

167 thickness of the sample slice is small compared to its width (1/4 to 1/22), diffusion was
168 considered to be essentially one-dimensional. Using the relative decrease of the integral
169 absorbance of OH and OD regions, diffusion coefficients can be calculated using Fick's
170 second law for one-dimensional diffusion in an infinite plate with a homogenous initial
171 concentration (Carslaw and Jaeger 1959; Ingrin et al. 1995).

172 For decreasing concentrations during H-D or D-H exchange experiments, the average
173 concentration measured across the slice thickness is described by the following equation:

174 $$\frac{C_{av}(t)}{C_0} = \frac{8}{\pi^2}\sum_{n=0}^{\infty}\frac{1}{(2n+1)^2}\exp\left(\frac{-Dt(2n+1)^2\pi^2}{4L^2}\right) \quad (1)$$

175 where C_0 is the initial value of the integrated absorbance, $C_{av(t)}$ the integrated
176 absorbance at annealing time t, D the diffusion coefficient, L the half thickness of the
177 slice.

178 For increasing concentrations during the H-D or D-H exchange experiments, the
179 following equation was employed (C_s represents the concentration at saturation at the
180 conditions of the experiments):

181 $$\frac{C_{av}(t)}{C_s} = 1 - equation\ (1) \quad (2)$$

182 The diffusion coefficient D was determined by numerically fitting the relative
183 concentration of C/C_0 (the ratio of integral absorbances A/A_0) and C/C_s (the ratio of A/A_s,

where, as described in the text later, only the defects available for the exchange are considered) against *t* for the decreasing and increasing species, respectively. It was assumed that the diffusion coefficient does not change with concentration of OH species. Since it has been shown in previous studies that hydrogen diffusion in garnets is isotropic (Ingrin and Blanchard 2006), we assumed the same is true for H-D exchange in andradite.

Activation energy was obtained by fitting the diffusion coefficients to an Arrhenius law:

$$D = D_0 \exp(-\frac{E_a}{kT}) \quad (3)$$

Where D_0 is the diffusivity at infinite temperature and E_a is the activation energy.

Results

Figure 2 shows a representative spectrum of andradite SER13, and the evolution of FTIR absorption during H-D exchange at 500 °C. As shown in Figure 2, the most prominent OH absorption bands are located at 3612, 3583, 3564 cm^{-1} and a minor band is found at 3634 cm^{-1}. These OH absorptions are typical of andradite from a skarn (Amthauer and Rossman 1998), and resemble the Ti-bearing andradite described by Armbruster et al. (1998) and the KPK 54-9 andradite An_{99} from Phu Kha Hill, Thailand used by Phichaikamjornwut et al. (2012) to study hydrogen dehydration and rehydration. Using Gaussian and Lorentzian (for bands at 3641 and 3526 cm^{-1}) shapes, spectral

peak-deconvolution using Peakfit software (SPSS Inc.) leads to 12 different peaks located at 3641, 3634, 3628, 3621, 3612, 3605, 3596, 3583, 3575, 3564, 3547, 3526 and a small broad band of water at 3406 cm^{-1}, probably due to the presence of some fluid inclusions (Fig. 3a). The deconvolution of the weakest bands is guided by the results of the dehydration experiments of Kurka et al. (2005) and in-situ IR experiments at varying temperatures down to -150 °C (unpublished data). The deconvolution of the corresponding OD absorption bands is also shown in Figure 3b.

The observed frequency shift due to the isotopic replacement (ν_{OH}/ν_{OD} close to 1.355) is in agreement with previous observations in anhydrous minerals and hydrates during H-D exchange (Hercule and Ingrin, 1999; Blanchard and Ingrin 2004a; Kurka et al. 2005; Mikenda, 1986).

At first glance, the shape and relative absorbances of OD bands appear similar to the OH bands and do not change during annealing, which is a regular behavior observed for H-D exchange in minerals (Ingrin and Blanchard 2006). The match between OH and OD bands is perfect for the majority of bands. However, a closer look at the spectra shows that the OH bands at 3634 cm^{-1} and 3628 cm^{-1}, which are coupled respectively with OD bands at 2680 cm^{-1} and 2677 cm^{-1}, have a different behavior (Fig. 4). The intensity of the OH band at 3634 cm^{-1} decreases continuously during the exchange until it almost disappears while the band at 3628 cm^{-1} shows a more limited decrease. The

lower-frequency OD absorption band at 2677 cm^{-1} is the first to appear during exchange. The intensity of this band increases but the final magnitude of this band is lower than that of the higher-frequency band at 2680 cm^{-1} (Fig. 4a, b). Figure 5 shows the quantitative evolution of these four bands (3634, 3628, 2680 and 2677 cm^{-1}) and the two associated H-defects. The evolution of the associated H-defects can be followed by plotting the evolution of the sum of OH and OD integral absorbances, taking into account the difference of the extinction coefficients of the two isotopes ($A_{OH} + \beta A_{OD}$; see more explanations in the description of Table 3 below). The interesting feature is that the total concentration of the defects associated with the two bands remains constant throughout the experiment and only their relative proportions adjust during the exchange (sum of the absorbances, Fig. 5c). This suggests that the two defects are probably two different configurations (giving rise to lower-frequency and higher-frequency bands) of the same defect, albeit with very similar energies. It was not possible to correlate the final ratio of the two bands with annealing temperature or their initial ratio. The particular behavior of these four bands shows that some local adjustments occur during annealing, but that this does not affect the overall diffusion process nor the measured diffusion coefficients.

Another important specific feature of H-D exchange in andradite is that, like for the extraction experiments performed earlier (Kurka 2005, Phichaikamjornwut et al. 2012), the exchange never reaches completion. We find that even at the end of the H-D

exchange experiments, the original OH bands remain evident on the spectra, albeit at reduced (15 to 35 %) intensities (Table 3). Even if the annealing time is prolonged by a factor of 4, the absorbance intensities of the OH and OD bands remain constant within uncertainties.

As the absorbance of OH bands (A_{OHf}) at the final stage of the exchange is not zero, the corresponding amount of H-defects were considered unavailable for the H-D exchange. Thus, for the exchange we only considered the H-defects corresponding to the difference between the initial absorbance, at time $t = 0$ and the final absorbance (A_{OH0} - A_{OHf}) when a steady state was reached (Table 3). Therefore, the evolution with time (t) of the intensities of OH and OD bands during H-D exchange is best represented by the normalized values: $(A_{OH} - A_{OHf})/(A_{OH0} - A_{OHf})$ and A_{OD}/A_{ODf} (Table 3); where A_{OH} and A_{OD} are the integral absorbances of the OH and OD bands at time t, and A_{ODf} is the integral absorbance of the OD bands at the final stage of exchange when A_{OD} has reached a steady state maximum value (Table 3). For reverse experiments (D-H exchanges experiments) the evolution with time is represented by the normalized values: $(A_{OH} - A_{OH0})/(A_{OHf} - A_{OH0})$ and A_{OD}/A_{OD0}; where A_{OH0} and A_{OD0} are the integral absorbances of the bands at the beginning of the D-H exchange (t = 0) and A_{OHf} is the value of A_{OH} at the end of D-H exchange. The last column of Table 3 shows the value of $(A_{OH} + \beta A_{OD})$, where β is the ratio of the extinction coefficient of OH and OD ($\varepsilon_{OH}/\varepsilon_{OD}$). $(A_{OH} + \beta A_{OD})$ represents the

259 total concentration of H-defects present in the sample for the H-D exchange. β is deduced
260 from the value (A_{OH0} - A_{OHf})/A_{ODf} for each H-D exchange. An average value of 1.66 ±
261 0.03 was measured. The almost constant value of (A_{OH} + βA_{OD}), which accounts to the
262 total value of integral absorbance of OH and OD bands, indicates that there is no loss of
263 hydrous species during the experiments. It must be also noted that, at the end of two D-H
264 exchange experiments (SER04 and SER13), the exchange is complete with A_{OD} almost at
265 zero.

266 The evolution with time (*t*) of the normalized values of the H-D and D-H are presented
267 in Figure 6. For each experiment, a diffusion coefficient *D* is deduced from the fit by
268 equation (1) for the decreasing species and equation (2) for the increasing species (solid
269 line; Fig. 6). The error bars on *D* are estimated from the extreme values that still fit the
270 data within the experimental uncertainties (dashed lines; Fig. 6). The diffusion
271 coefficients deduced from the two reverse experiments (D-H exchange) are close to those
272 calculated after H-D exchange. This suggests that the kinetics of both processes are the
273 same (Table 2; Fig. 6).

274 A complete restoration of OH band intensities after D-H exchange (rehydration)
275 demonstrates the reversibility of the exchange experiments. Because data on the integral
276 absorbance ratio vs. *t* plot only slightly fluctuate around an equilibrium value (Fig. 6), we
277 consider that a steady-state was reached at the end of the exchange experiments. The

intensities of all absorption bands follow the same kinetics regarding exchange of H by D or D by H. The calculated diffusion coefficients, listed in table 2, are fitted to an Arrhenius law (Fig. 7). Following the least-square cubic method proposed by York (1966), the least-square fits lead to the diffusion law:

$$D = D_0 \exp\left[-\frac{(96 \pm 11) kJ/mol}{RT}\right] \quad (4)$$

with $\log D_0$ (in m^2/s) = -5.9 ± 0.7.

Overall uncertainties correspond to the sum of those associated with the least-square fitting, T (fixed at 5 °C) and the individual uncertainties on D.

The diffusion coefficients deduced from the two points of SER16 (P3 and P6) are similar within the uncertainty of the experiments ($2.0 \pm 1.0\ 10^{-12}$ and $1.3 \pm 1.2\ 10^{-12}$ m^2s^{-1}, resp.). This confirms that the kinetics of H-D exchange is not strongly dependent on the concentration of H-defects. H-D and D-H experiments performed in a same slice also show that the kinetics of the reverse experiment is not affected by the duration of the previous H-D experiment. Fast D-H exchange starts immediately when annealing in a D-rich atmosphere (see SER04 experiments, Table 3). This demonstrates that the incomplete exchange in the H-D experiment is not due to a slowdown of the exchange kinetics, which may be linked to a dependence of the diffusion coefficient with H concentration, but that a steady-state is reached for the exchange. These results suggest

296 that a fraction of the H in the structure (15-30%) was not accessible for the H-D exchange.
297 The shape of the OH spectrum at the end of the H-D exchange experiments is identical to
298 that of the original spectrum (Figs. 2 & 4), except for the small changes affecting the
299 bands at 3634 and 3628 cm^{-1}. Thus, the fraction of H not accessible for H-D exchange is
300 not linked to a specific H-defect but affect all types of OH bands. The complete
301 rehydrogenation (SER04 and SER13) shows that no irreversible change occurs in the
302 sample during annealing (Fig. 2, Table 3). Slices with different thicknesses, performed at
303 the same temperature (SER 04 and SER15 at 600 ˚C; SER13 and SER19 at 500 ˚C), give
304 similar diffusion coefficients. This illustrates that there is no systematic dependence of
305 diffusion related to the thickness of the sample.

306 **Discussion**

307 **Comparison with H diffusion laws in NAMs**

308 Figure 8 shows a comparison between the diffusion laws for H-D exchange in
309 andradite and several other NAMs. The activation energy of andradite (96 ± 11 kJ/mol) is
310 amongst the lowest amongst all hydrogen diffusion in NAMs. The activation energies for
311 H-D exchange in NAMs are in the range 100-190 kJ/mol (grossular $Gr_{83}An_{14}$: 102 kJ/mol,
312 Kurka et al. 2005; grossular $Gr_{73}An_{23}$: 190 kJ/mol, Kurka 2005; Dora Maria pyrope: 140
313 kJ/mol, Blanchard and Ingrin 2004a; diopside: 145 kJ/mol, Hercule and Ingrin 1999;
314 olivine // a: 140 kJ/mol, Du Frane et al. 2012; forsterite // c: 134 kJ/mol, Ingrin and

315 Blanchard (2006); quartz // c: 176 kJ/mol, Kats et al. 1962). The data we present here
316 show that H-D exchange in andradite is the fastest of all NAMs and, at 700 °C, it is two
317 orders of magnitude faster than in other garnets (Fig. 8). H-D exchange data are generally
318 assumed to represent the mobility of hydrogen as a single proton hopping from one
319 oxygen site to another (see for instance, Hercule and Ingrin 1999 and Ingrin et al. 2001).
320 Because, the activation energy of hydrogen diffusion in andradite is comparable to other
321 NAMs we suggest that a similar mechanism for hydrogen diffusion is highly probable.

322

323 **Comparison with extraction/incorporation laws in andradite and garnets of the**
324 **grossular-andradite series**

325 Figure 9a shows the chemical diffusion coefficients for H as calculated from
326 extraction experiments in andradite with similar compositions to those described here
327 (An_{99}) compared to the results of H-D and D-H exchanges (Kurka 2005; Ingrin and
328 Blanchard 2006; Phichaikamjornwut et al. 2012). Extraction experiments in air show at
329 least two distinct diffusivities: hydrogens associated with bands at frequencies below
330 3580 cm^{-1} have a faster diffusion law than the ones associated with bands at frequencies
331 above 3600 cm^{-1} (laws I and II respectively; Fig. 9). The activation energies of the
332 extraction laws are higher than those of the H-D exchange (271 and 209 kJ/mol,
333 respectively compared to 96 kJ/mol). This is common in garnets (Kurka 2005; Ingrin and

Blanchard, 2006). The diffusivities for H-extraction in An_{99} are one to three orders of magnitude lower than the diffusivity deduced from H-D exchange at 800 °C. This means that in An_{99} the process of chemical diffusion involved in H-extraction experiments in air at temperatures below 1000 °C is not limited by H diffusion, but by a slower mechanism (Fig. 9). An interesting point is that in H-incorporation experiments in H_2 at 700 and 800 °C, on the same slices as were used for H-extraction in air, Phichaikamjornwut et al. (2012) observed a diffusion rate of one to two orders of magnitude faster than for extraction (empty square compared to solid squares in Fig. 9a). The values measured by Phichaikamjornwut et al. (2012) are lower limits since both slices were completely rehydrogenated after the first annealing step (steps of 20 minutes and 1h, respectively). This suggests that the mechanism that controls H incorporation must be different from the one controlling extraction and that H incorporation is potentially fast enough to be limited by the mobility of hydrogen as defined by the diffusion law deduced from H-D exchange. Phichaikamjornwut et al. (2012) also showed that the kinetics of H incorporation are faster than kinetics of extraction for other compositions in the grossular-andradite series where iron exists mostly as Fe^{3+} (Fig. 9b). The activation energies for H-extraction in these garnets are also high compared to the activation energies for H diffusion, 96 – 102 kJ/mol against around 320 – 340 kJ/mol (An_{14}: $Gr_{83}An_{14}$, 323 kJ/mol, Kurka et al. 2005; An_{20} -An_{45}: 338 kJ/mol, Phichaikamjornwut et al. 2012). It is interesting to note that hydrogen diffusivity in the grossular-andradite series increases dramatically with the

354 andradite component, i.e., by two orders of magnitude from An_{14} to An_{99} (Fig. 9b). Since
355 no H-D exchange experiments have been conducted on intermediate compositions it is
356 difficult to say if the rate of diffusion evolves smoothly with the andradite content or if a
357 sharp increase occurs at a critical composition.

358 In their study of H-extraction in andradite Phichaikamjowut et al. (2012) explained the
359 apparent decrease of the dehydrogenation rate in long experiments by two effects: a
360 dependence of diffusion rate with hydrogen concentration (Wang et al. 1996) and
361 different kinetics for the different OH bands that compose the IR spectra (Kurka et al.
362 2005). These two effects can significantly affect the kinetics of H-extraction, but they
363 cannot explain why the same phenomenon is observed in H-D exchange. The
364 concentration of hydrous defects remains constant and the relative behavior of the OH
365 bands are similar during exchange experiments. The fraction of H-defects that does not
366 participate to the H-D exchange (15 to 35%) cannot be associated with a specific defect
367 since overall shape of the spectrum remains the same during the exchange. These
368 hydrogens must be dispersed in the bulk of the sample: the proportion of these “relict”
369 hydrogens and the quality of the fit of the H-D exchange by a single diffusion process are
370 independent of the thickness of the slices (Fig. 6). The exact nature of these
371 heterogeneities in andradite (clustering of H-defects, presence of 2D or 3D defects …) is
372 not completely understood but they are good candidates to explain the specific behavior

373 observed during H-extraction experiments in andradite-rich garnets by previous authors
374 (Kurka 2005; Phichaikamjorn et al. 2012).

375 The exact mechanisms of H-extraction and H-incorporation in andradite are still
376 unknown. Phichaikamjornwut et al. (2012) have shown that the redox-reaction Fe^{2+} +
377 $OH^- = Fe^{3+} + O^{2-} + 1/2H_2$ alone cannot control H-extraction, since most of the time there
378 is not enough Fe^{2+} available in the crystal to remove all the hydrogen atoms. However,
379 there is plenty of Fe^{3+} available for the reverse reaction and H-incorporation. This process
380 may explain why H-incorporation is generally faster than H-extraction in andradite and
381 why the reaction is limited by the mobility of hydrogen. Even if Phichaikamjornwut et al.
382 (2012) did not find evidence for the reduction of Fe^{3+} into Fe^{2+} after Mössbauer
383 measurements, the presence of Fe^{3+} is well known to provide a suitable charge balance
384 mechanism and pathways during rehydrogenation.

385 Determining absolute hydrogen concentrations in andradite is highly problematic
386 because no specific calibration exists. We used an average value of 0.18 ± 0.12 wt % H_2O
387 in this andradite. This means that it is also difficult to estimate the contribution of Fe^{2+}
388 and others multivalent cations such as Mn in the mechanism of H-extraction. Despite this,
389 the potential role of minor cations in the extraction process of hydrogen in andradite
390 should not be underestimated. Electrical conductivity in pyrope-almandine garnets is
391 generally assumed to be controlled by the mobility of small polarons (Day et al. 2012).

However, the activation energy of conductivity is much lower than the activation energy of H-extraction (120-130 $kJmol^{-1}$; Dai et al. 2012, 2013 compared to 200-300 $kJmol^{-1}$). Therefore, because redox reactions cannot alone explain the chemical diffusion of hydrogen in garnet, another process, with a higher activation energy, must be involved. Diffusion of cation vacancies is a good candidate for the control of this process. It is known that the activation energies for cation diffusion on the X site of garnets (Ca, Fe, Mg, Mn) are comparable to the activation energy of H-extraction (230 – 300 $kJmol^{-1}$; Carlson 2006; Ganguly 2010). Therefore, it is possible that the mobility of this type of cation vacancies controls H-extraction in andradite. However, because the number of experiments performed on andradite is limited, many issues remain to be answered. We do not know, for example, if the extraction kinetics remains the same after a full cycle of H-extraction and H-incorporation on the same sample. If, for example, the first H-extraction required that cations reorganized around the defects to allow local charge balance after H removal (for instance, Mn diffusion to a neighbor site), then no subsequent reorganization would be needed for the second extraction experiment.

Implications for the preservation of isotopic signatures

The present results suggest that the kinetics of H-D exchange in andradite are much faster than for other NAMs, and significantly faster than for other garnets (Fig. 8). This

means that the capacity of andradite to retain hydrogen isotropic evidence of fluid-rock interaction is weaker than in other garnets. Using the diffusion law calculated here, the isotope ratio in the center of a 5 cm diameter andradite grain would not survive more than; 1) few months at a temperature of 600 °C, 2) 10 years at 400 °C and 3) less than 30000 years at 200 °C. Therefore, we suggest that the hydrogen isotope signature in andradite can only be relied upon to record low-grade metamorphic and metasomatic events, mostly short events at shallow depth and below 400 °C. At higher temperatures and in deeper events, the ability of any garnet to retain isotopic information will strongly depend on its andradite content: a change of composition from $Gr_{86}An_{14}$ to An_{99}, will have the same effect on H mobility as a temperature increase of 500 °C (see the shift of diffusion laws in Fig. 9b). The same effect is expected to control the closure temperature of garnet for hydrogen isotopes.

It is essential to consider the results of H-D diffusion experiments in any discussion of the isotopic signature of garnets because hydrogen diffusion through garnet is always faster than the chemical diffusion. In addition, these differences become more apparent at lower temperatures due to the difference of the activation energies. The fast diffusion of hydrogen in garnet may explain the large heterogeneous δD values and the different behavior they exhibit when compared to $\delta^{18}O$ values (Zheng et al. 2003; Chen et al. 2011; Sheng et al. 2007). More data from H-D exchange experiments on garnets of various

compositions are needed to better understand the significance of any measured isotopic signature (Gong et al. 2007).

Acknowledgments

This work was supported by National Natural Science Foundation of China (No. 41225005) and China Scholarship Council. We thank Kevin Grant, Henrik Skogby and an anonymous reviewer for their helpful suggestions to improve the manuscript.

References cited

Amthauer, G., and Rossman, G.R. (1998) The hydrous component in andradite garnet. American Mineralogist, 83, 835-840.

Armbruster, T., and Geiger, C.A. (1993) Andradite crystal chemistry, dynamic X-site disorder and structural strain in silicate garnets. European Journal of Mineralogy, 5, 59-71.

Armbruster, T. (1995) Structure refinement of hydrous andradite, $Ca_3Fe_{1.54}Mn_{0.20}Al_{0.26}(SiO_4)_{1.65}(O_4H_4)_{1.35}$, from the Wessels mine, Kalahari manganese field, South Africa. European Journal of Mineralogy, 7, 1221-1225.

Armbruster T., Birrer J., Libowitzky E., and Beran A. (1998) Crystal chemistry of Ti-bearing andradites. European Journal of Mineralogy, 10, 907-921.

448 Bell, D.R., and Rossman, G.R. (1992a) Water in Earth's mantle: The role of nominally
449 anhydrous minerals. Science, 255, 1391-1397.

450 Bell, D.R., and Rossman, G.R. (1992b) The distribution of hydroxyl in garnets from the
451 subcontinental mantle of southern Africa. Contributions to Mineralogy and Petrology,
452 111, 161-178.

453 Blanchard, M., and Ingrin, J. (2004a) Kinetics of deuteration in pyrope. European Journal
454 of Mineralogy, 16, 567-576.

455 Blanchard, M., and Ingrin, J. (2004b) Hydrogen diffusion in Dora Maira pyrope. Physics
456 and Chemistry of Minerals, 31, 593-605.

457 Carlson, W.D. (2006) Rates of Fe, Mg, Mn and Ca diffusion in garnet. American
458 Mineralogist, 91, 1-11.

459 Carslaw, H.S., and Jaeger, J.C. (1959) Conduction of Heat in Solids, 510 p. Clarendon,
460 Oxford, UK.

461 Chen, R.X., Zheng, Y.F., and Gong, B. (2011) Mineral hydrogen isotopes and water
462 contents in ultrahigh-pressure metabasite and metagranite: Constraints on fluid flow
463 during continental subduction-zone metamorphism. Chemical Geology, 281, 103-124.

464 Cho, H., and Rossman, G.R. (1993) Single crystal NMR studies of low-concentration
465 hydrous species in minerals: grossular garnet. American Mineralogist, 78, 1149-1164.

466 Cohen-Addad, C., Ducros, P., and Bertaut, E.F. (1967) Étude de la substitution du
467 groupement SiO_4 par $(OH)_4$ dans les composés $Al_2Ca_3(OH)_{12}$ et
468 $Al_2Ca_3(SiO_4)_{2.16}(OH)_{3.36}$ de type grenat. Acta Crystallographica, 23, 220-230 (in
469 French).

470 Dai, L., Li H., Hu, H., Shan, S., Jiang, J., and Hui, K. (2012) The effect of chemical
471 composition and oxygen fugacity on the electrical conductivity of dry and hydrous
472 garnet at high temperatures and pressures. Contribution to Mineralogy and Petrology,
473 163, 689-700.

474 Dai, L., Li H., Hu, H., Jiang, J., Hui, K., and Shan, S. (2013) Electrical conductivity of
475 Alm82Py15Grs3 almandine-rich garnet determined by impedance spectroscopy at
476 high temperatures and high pressures. Tectonophysics, 608, 1086-1093.

477 Du Frane, W.L., and Tyburczy, J.A. (2012) Deuterium-hydrogen exchange in olivine:
478 Implications for point defects and electrical conductivity. Geochemistry, Geophysics,
479 Geosystems, 13, 3.

480 Forneris, J.F., and Skogby, H. (2004) Is hydrogen loss via ion oxidation an important
481 mechanism in nominally anhydrous minerals? Geochimica et Cosmochimica Acta, 68,
482 11, Suppl. 1, 35.

Ganguly, J. (2010) Cation diffusion kinetics in aluminosilicate garnets and geological applications. In Y. Zhang and D.J. Cherniak, Eds.,Diffusion in minerals and melts, 72, p. 559-601, Reviews in Mineralogy and Geochemistry, Mineralogical Society of America, Chantilly, Virginia.

Gong, B., Zheng, Y.F., and Chen, R.X. (2007) TC/EA-MS online determination of hydrogen isotope composition and water concentration in eclogitic garnet. Physics and Chemistry of Minerals, 34, 687-698.

Hercule, S., and Ingrin, J. (1999) Hydrogen in diopside: Diffusion, kinetics of extraction-incorporation and solubility. American Mineralogist, 84, 1577-1587.

Ingrin, J., and Blanchard, M. (2006) Diffusion of hydrogen in minerals. In H. Keppler and J.R. Smyth, Eds.,Water in Nominally Anhydrous Minerals, 62, p. 291-320, Reviews in Mineralogy and Geochemistry, Mineralogical Society of America, Chantilly, Virginia.

Ingrin, J., and Skogby, H. (2000) Hydrogen in nominally anhydrous upper-mantle minerals: concentration levels and implications. European Journal of Mineralogy, 12, 543-570.

Ingrin, J., Hercule, S., and Charton, T. (1995) Diffusion of hydrogen in diopside: results of dehydration experiments. Journal of Geophysical Research, 100, 15489-15499.

501 Ingrin, J., Pacaud, L., and Jaoul, O. (2001) Anisotropy of oxygen diffusion in diopside.
502 Earth and Planetary Science Letters, 192, 347-361.

503 Kats, A., Haven. Y., and Stevels, J.M. (1962) Hydroxyl groups in α-quartz. Physics and
504 Chemistry of Glasses, 3, 69-76.

505 Kobayashi, S., and Shoji, T. (1987) Infrared spectra and cell dimensions of
506 hydrothermally synthesized grandite-hydrograndite series. Mineralogical Journal, 13,
507 490-499.

508 Kurka, A. (2005) Hydrogen in Ca-rich Garnets: diffusion and Stability of OH-defects,
509 145 p. Ph.D. thesis, Université de Toulouse, France.

510 Kurka, A., Blanchard, M., and Ingrin, J. (2005) Kinetics of hydrogen extraction and
511 deuteration in grossular. Mineralogical Magazine, 69, 359-371.

512 Lager, G.A., Armbruster, T., and Faber, J. (1987) Neutron and X-ray diffraction study of
513 hydrogarnet $Ca_3Al_2(O_4H_4)$. American Mineralogist, 72, 756-765.

514 Lager, G.A., Armbruster, T., Rotella, F.J., and Rossman, G.R. (1989) The OH
515 substitution in garnets: X-ray and neutron diffraction, infrared, and
516 geometric-modeling studies. American Mineralogist, 74, 840-851.

517 Libowitzky, E., and Rossman, G.R. (1997) An IR absorption calibration for water in
518 minerals. American Mineralogist, 82, 1111-1115.

519 Locock, A., Luth, R.W., Cavell, G.G., Smith, D.G.S., and Duke, M.J.M. (1995)
520 Spectroscopy of the cation distribution in the schorlomite species of garnet. American
521 Mineralogist, 80, 27-38.

522 Maldener, J., Ho □sch, A., Langer, K., and Rauch, F. (2003) Hydrogen in some natural
523 garnets studied by nuclear reaction analysis and vibrational spectroscopy. Physics and
524 Chemistry of Minerals, 30, 337-344.

525 Matveev, S., O'Neill, H.St.C., Ballhaus, C., Taylor, W.R., and Green, D.H. (2001) Effect
526 of silica acitivity on OH− IR spectra of olivine: Implications for low $aSiO_2$ mantle
527 metasomatism. Journal of Petrology, 42, 721-729.

528 Mikenda,W. (1986) Stretching frequency versus bond distance correlation of
529 O–D(H)…Y(Y = N, O, S, Se, Cl, Br, I) hydrogen bonds in solid hydrates. Journal of
530 Molecular Structure, 147, 1-15.

531 Phichaikamjornwut, B., Skogby, H., Ounchanum, P., Limtrakun P., and Boonsoong, A.
532 (2012) Hydrous components of grossular-andradite garnets from Thailand: thermal
533 stability and exchange kinetics. European Journal of Mineralogy, 24, 107-121.

534 Rossman, G.R., and Aines R.D. (1991) The hydrous components in garnets:
535 grossular-hydrogrossular. American Mineralogist, 76, 1153-1164.

536 Sheng, Y.M., Xia, Q.K., Dallai, L., Yang, X.Z., and Hao, Y.T. (2007) H_2O contents and
537 D/H ratios of nominally anhydrous minerals from ultrahighpressure eclogites of the
538 Dabie orogen, eastern China. Geochimica et Cosmochimica Acta, 71, 2079-2103.

539 Thompson, A.B. (1992) Water in the Earth's upper mantle. Nature, 358, 295-302.

540 Wang, L., Zhang, Y., and Essene, E. (1996) Diffusion of the hydrous component in
541 pyrope. American Mineralogist, 81, 706-718.

542 Xia Q.K., Sheng Y.M., Yang X.Z., and Yu H.M. (2005) Heterogeneity of water in garnets
543 from 655 UHP eclogites, eastern Dabieshan, China. Chemical Geology, 224, 237-246.

544 York, D. (1966) Least-squares fitting of a straight line. Canadian Journal of Physics, 44,
545 1079-1086.

546 Zheng, Y.F., Fu, B., Gong, B., and Li, L. (2003) Stable isotope geochemistry of ultrahigh
547 pressure metamorphic rocks from the Dabie-Sulu orogen in China: implications for
548 geodynamics and fluid regime. Earth Science Reviews, 62, 105-161.

549

550 **Figure captions:**

551

552 Figure 1. Examples showing the baseline correction of OH and OD absorption regions:
553 **(a)** OH stretch region (3750 to 3150 cm^{-1}); Slice SER18, annealed at 700 ˚C, with a

554 thickness (2L) of 596 μm and **(b)** OD stretch region (2700 to 2500 cm^{-1}); Slice SER16,
555 annealed at 550 ˚C, with a thickness (2L) of 236 μm.

556 Figure 2. Representative evolution of andradite spectra after annealing under Ar/D_2
557 atmosphere, showing the replacement of OH bands by OD bands. Slice SER13, annealed
558 at 500 ˚C, with a thickness (2L) of 273 μm. The uppermost spectrum shows the result
559 after rehydrogenation in Ar/H_2 atmosphere at 400 °C.

560 Figure 3. Representative IR absorbance spectra of the **(a)** OH and **(b)** OD stretching
561 regions of andradite. Deconvolution of the spectra yields 12 OH and OD peaks. Slice
562 SER17, with a thickness (2L) of 182 μm.

563 Figure 4. Detail of how spectra evolve during annealing. Spectra show the specific
564 behavior of **(a)** OH bands at 3634 and 3628 cm^{-1}, where length of annealing time
565 increases with decreasing bands intensities **(b)** corresponding OD bands at 2680 and 2677
566 cm^{-1}, where time of annealing experiment increases with increasing bands intensities.
567 Slice SER13, annealed at 500 ˚C, with a thickness (2L) of 273 μm.

568 Figure 5. Evolution of the integral absorbance of **(a)** OH bands at 3628 and 3634 cm^{-1},
569 **(b)** corresponding OD bands at 2677 and 2680 cm^{-1} and **(c)** the sum of OH and OD bands
570 ($A_{OH} + \beta A_{OD}$) with length of annealing time . Slice SER13, annealed at 500 ˚C.

Figure 6. Fits of data by equation (1) and (2) for H-D and D-H experiments conducted at temperatures between 400 and 700 ˚C (continuous line). Empty circles represent the evolution of increasing species: OD bands for H-D exchange (resp. OH bands for D-H exchange). Solid circles represent the evolution of decreasing species: OH bands for H-D exchange (resp. OD bands for D-H exchange). Error bars on D are deduced from the range of D values that still fit the data (discontinuous lines)

Figure 7. Arrhenius plot showing diffusion data for H-D and D-H exchange and the associated fit law.

Figure 8. Compilation of diffusion laws for H-D exchange in NAMs. $Gr_{83}An_{14}$: Kurka et al. (2005); $Gr_{73}An_{23}$: Kurka (2005); Dora Maira pyrope: Blanchard and Ingrin (2004a); diopside: Hercule and Ingrin (1999); olivine // a: Du Frane et al. (2012); forsterite // c: Ingrin and Blanchard (2006); quartz // c: Kats et al. (1962); An_{99}: this study.

Figure 9. Comparison of H-D exchange kinetics with H-extraction and H-incorporation kinetics in **(a)** An_{99} and **(b)** the grossular-andradite series. Solid and empty squares correspond to the H-extraction and H-incorporation data of An_{99} while solid and empty circles correspond to the H-extraction and H-incorporation data of An_{20}-An_{45}, respectively from Phichaikamjornwut et al. (2012). The gray lines represent H diffusion laws deduced from H-D exchange experiments (An_{14}: $Gr_{83}An_{14}$, Kurka et al. 2005; An_{99}: this study); the black lines represent H diffusion laws deduced from

H-extraction experiments (An_{14}: $Gr_{83}An_{14}$, Kurka et al. 2005; An_{20}–An_{45}, Phichaikamjornwut et al. 2012; An_{99} I (lower-frequency bands), II (higher-frequency bands): Kurka 2005). The smaller squares are the original data when taking overall OH bands as a whole while the larger squares are the distinct data after separating OH bands into higher-frequency and lower-frequency bands. Arrows in (a) indicate that these values are probably underestimated.

598 **Tables:**

599 Table 1. Composition of andradite used in this study.

	EMPA	LA-ICP-MS
SiO_2	35.24 (0.51)	35.21 (0.50)
TiO_2	0.00	0.00
Al_2O_3	0.00	0.04 (0.06)
Cr_2O_3	0.02 (0.03)	0.00
Fe_2O_3	31.30 (0.54)	30.99 (0.24)
FeO	0.10 (0.26)	0.00
MnO	0.11 (0.06)	0.09 (0.006)
MgO	0.00	0.01 (0.00)
CaO	33.01 (0.41)	32.74 (0.36)
H_2O*	0.18 (0.12)	0.18 (0.12)
Total	99.96	99.26

Notes: H_2O* is estimated from FTIR measurement using different calibrations (see "Infrared analysis"). Standard deviations are indicated in parentheses.

600

601 Table 2. Summary of diffusion coefficients for H-D and D-H exchanges

Sample No.	T (°C)	Run duration (h)	Experiments	D (m^2s^{-1})
SER04	600	63.00	H-D exchange	$(4.5 \pm 2.5) \times 10^{-12}$
SER04	600	14.00	D-H exchange	$(5.5 \pm 3.0) \times 10^{-12}$
SER13	500	64.00	H-D exchange	$(4.5 \pm 1.0) \times 10^{-13}$
SER13	400	178.00	D-H exchange	$(4.5 \pm 1.5) \times 10^{-14}$
SER13	550	64.10	H-D exchange	$(9.5 \pm 2.0) \times 10^{-13}$
SER15	600	183.25	H-D exchange	$(6.0 \pm 2.5) \times 10^{-13}$
SER16-P3	550	8.07	H-D exchange	$(2.0 \pm 1.0) \times 10^{-12}$
SER16-P6	550	8.07	H-D exchange	$(1.3 \pm 1.2) \times 10^{-12}$
SER17	425	153.32	H-D exchange	$(3.3 \pm 1.3) \times 10^{-14}$
SER18	700	16.00	H-D exchange	$(7.5 \pm 2.5) \times 10^{-12}$
SER19	500	32.00	H-D exchange	$(8.0 \pm 3.5) \times 10^{-13}$

602 *Note*: The error bars on *D* are estimated from the extreme values deduced from Fig. 6. H-D exchange was
603 conducted with a gas mixture of $Ar_{(90\%)}/D_{2(10\%)}$ flowing through 99.9% D_2O and D-H exchange with a gas
604 mixture of $Ar_{(90\%)}/H_{2(10\%)}$ flowing through deionized H_2O.

605
606

607 Table 3. Experimental data from H-D and D-H exchange

H-D exchange						
t (h)	A_{OH}	A_{OD}	A_{OH}-A_{OHf}	(A_{OH}-A_{OHf})/(A_{OH0}-A_{OHf})	A_{OD}/A_{ODf}	A_{OH}+βA_{OD}
SER04; 600˚C; 2*L* = 277µm; size = 3.0 × 2.0 mm^2; A_{OH0}-A_{OHf} = 42.78-5.77 = 37.01; A_{ODf} = 22.42						
0.00	42.78	0.00	37.01	1.00	0.00	42.78
1.00	9.05	20.62	3.28	0.09	0.92	43.28
3.00	6.52	23.02	0.75	0.02	1.03	44.73
7.00	9.62	20.94	3.85	0.10	0.93	44.37
15.00	6.80	21.88	1.03	0.03	0.98	43.13
31.00	5.77	22.42	0.00	0.00	1.00	42.98
63.00	6.30	22.28	0.53	0.01	0.99	43.28
SER13; 500˚C; 2*L* = 273µm; size = 3.0 × 2.0 mm^2; A_{OH0}-A_{OHf} = 60.13-10.78 = 49.35; A_{ODf} = 29.81						
0.00	60.13	0.00	49.35	1.00	0.00	60.13
1.00	44.50	9.40	33.72	0.68	0.32	60.10
2.00	38.58	13.62	27.80	0.56	0.46	61.19
4.00	27.30	19.91	16.52	0.33	0.67	60.35
8.00	17.56	25.29	6.78	0.14	0.85	59.54
16.00	11.60	28.98	0.82	0.02	0.97	59.71
32.00	10.78	29.81	0.00	0.00	1.00	60.26
64.00	11.33	29.16	0.55	0.01	0.98	59.74
SER13; 550˚C; 2*L* = 273µm; size = 3.0 × 2.0 mm^2 (second annealing); A_{OH0}-A_{OHf} = 57.92-17.05 = 40.87; A_{ODf} = 25.46						
0.00	57.92	0.30	40.87	1.00	0.00	58.42
0.50	48.87	6.69	31.82	0.78	0.25	59.98
1.00	41.71	11.10	24.66	0.60	0.43	60.14
2.00	29.88	17.45	12.83	0.31	0.68	58.85
4.00	21.08	23.17	4.03	0.10	0.91	59.54
8.00	18.23	25.05	1.18	0.03	0.98	59.81
16.10	24.88	21.34	7.83	0.19	0.84	60.30
32.10	19.84	23.90	2.79	0.07	0.94	59.51
64.10	17.05	25.46	0.00	0.00	1.00	59.31
SER15; 600˚C; 2*L* = 671µm; size = 3.2 × 2.4 mm^2; A_{OH0}-A_{OHf} = 159.87-33.54 = 126.33; A_{ODf} = 74.34						
0.00	159.87	0.00	126.33	1.00	0.00	159.87
0.50	138.01	12.30	104.47	0.83	0.17	158.43
1.00	129.85	19.46	96.31	0.76	0.26	162.15

2.00	121.94	24.99	88.40	0.70	0.34	163.42
4.00	117.57	26.71	84.03	0.67	0.36	161.91
8.00	100.83	38.74	67.29	0.53	0.52	165.14
16.00	80.84	51.13	47.30	0.37	0.69	165.72
32.00	53.74	64.27	20.20	0.16	0.86	160.43
64.25	37.63	68.89	4.09	0.03	0.93	151.99
105.25	33.54	74.34	0.00	0.00	1.00	156.94
183.25	40.71	67.40	7.17	0.06	0.91	152.59

SER16-P3; 550˚C; 2*L* = 236µm; size = 4.0 × 2.7 mm^2; A_{OH0}-A_{OHf} = 16.33-5.57 = 10.76; A_{ODf} = 6.32

0.00	16.33	0.00	10.76	1.00	0.00	16.33
0.50	11.24	3.16	5.67	0.53	0.50	16.49
1.00	8.36	4.50	2.79	0.26	0.71	15.83
2.07	5.65	6.32	0.08	0.01	1.00	16.14
4.07	5.93	6.22	0.36	0.03	0.98	16.26
8.07	5.57	6.32	0.00	0.00	1.00	16.06

SER16-P6; 550˚C; 2*L* = 236µm; size = 4.0 × 2.7 mm^2; A_{OH0}-A_{OHf} = 36.04-11.10 = 24.94; A_{ODf} = 14.58

0.00	36.04	0.00	24.94	1.00	0.00	36.04
0.50	27.56	5.46	16.46	0.66	0.37	36.62
1.00	21.40	8.87	10.30	0.41	0.61	36.12
2.07	12.87	13.47	1.77	0.07	0.92	35.23
4.07	11.96	14.18	0.86	0.03	0.97	35.50
8.07	11.10	14.58	0.00	0.00	1.00	35.30

SER17; 425˚C; 2*L* = 182µm; size = 4.5 × 4.0 mm^2; A_{OH0}-A_{OHf} = 42.30-15.58 = 26.72; A_{ODf} = 15.93

0.00	42.30	0.00	26.72	1.00	0.00	42.30
0.50	40.61	1.05	25.03	0.94	0.07	42.35
1.00	39.06	1.53	23.48	0.88	0.10	41.60
2.00	37.81	2.63	22.23	0.83	0.17	42.18
4.00	36.13	3.60	20.55	0.77	0.23	42.11
8.00	32.52	5.65	16.94	0.63	0.35	41.90
16.00	26.45	8.85	10.87	0.41	0.56	41.14
32.08	23.27	11.35	7.69	0.29	0.71	42.11
64.18	16.97	14.95	1.39	0.05	0.94	41.79
153.32	15.58	15.93	0.00	0.00	1.00	42.02

SER18; 700˚C; 2*L* = 596µm; size = 4.5 × 3.0 mm^2; A_{OH0}-A_{OHf} = 117.92-26.92 = 91.00; A_{ODf} = 53.71

0.00	117.92	0.00	91.00	1.00	0.00	117.92

1.00	61.99	35.80	35.07	0.39	0.67	121.42
2.00	44.24	45.59	17.32	0.19	0.85	119.92
4.00	27.97	53.13	1.05	0.01	0.99	116.17
8.00	29.72	51.98	2.80	0.03	0.97	116.01
16.00	26.92	53.71	0.00	0.00	1.00	116.08
SER19; 500˚C; 2*L* = 140µm; size = 5.0 × 2.8 mm^2; A_{OH0}-A_{OHf} = 34.17-9.69 = 24.48; A_{ODf} = 14.53						
0.00	34.17	0.00	24.48	1.00	0.00	34.17
0.50	22.85	6.62	13.16	0.54	0.46	33.84
1.00	18.68	9.44	8.99	0.37	0.65	34.35
2.00	15.05	11.46	5.36	0.22	0.79	34.07
4.00	12.32	13.05	2.63	0.11	0.90	33.98
8.12	10.83	14.05	1.14	0.05	0.97	34.15
32.00	9.69	14.53	0.00	0.00	1.00	33.81

D-H exchange

t (h)	A_{OH}		A_{OH}-A_{OH0}	(A_{OH}-A_{OH0})/(A_{OHf}-A_{OH0})	A_{OD}/A_{OD0}	A_{OH}+βA_{OD}
SER04; 600˚C; 2*L* = 277µm; size = 3.0 × 2.0 mm^2; A_{OHf}-A_{OH0} = 43.43-6.30 = 37.13; A_{OD0} = 22.28						
0.00	6.30	22.28	0.00	0.00	1.00	43.28
1.00	41.60	1.66	35.30	0.95	0.07	44.35
2.00	43.43	0.47	37.13	1.00	0.02	44.21
6.00	38.31	2.75	32.01	0.86	0.12	42.87
14.00	43.09	0.32	36.79	0.99	0.01	43.62
SER13; 400˚C; 2*L* = 273µm; size = 3.0 × 2.0 mm^2; A_{OHf}-A_{OH0} = 57.92-11.33 = 46.59; A_{OD0} = 29.16						
0.00	11.33	29.16	0.00	0.00	1.00	59.74
8.00	23.94	21.87	12.61	0.27	0.75	60.24
16.00	30.12	17.76	18.79	0.40	0.61	59.60
32.00	38.01	13.44	26.68	0.57	0.46	60.32
64.33	49.83	6.91	38.50	0.83	0.24	61.30
128.33	57.28	1.68	45.95	0.99	0.06	60.07
178.00	57.92	0.30	46.59	1.00	0.01	58.42

Notes: *t* is the time of annealing at nominal temperature; *2L* is the thickness of the slice; A_{OH} and A_{OD} are the integral absorbance of the OH and OD respectively; A_{OH0} and A_{OHf} are the integral absorbance of OH bands at $t = 0$ and at the final stage of exchange; A_{OD0} and A_{ODf} are the integral absorbances of OD bands at $t = 0$ and at the final stage of exchange, respectively; ($A_{OH} + \beta A_{OD}$) is the total integral absorbance considering both OH and OD bands adjusted by the ratio of the extinction coefficients $\beta = \varepsilon_{OH}/\varepsilon_{OD}$. *The two points of analysis P3 and P6 correspond to the concentration of the two sectors observed in SER16 (see text). It was used to test the possible impact of concentration on the result of H-D exchange.

615

This is a preprint, the final version is subject to change, of the American Mineralogist (MSA)
Cite as Authors (Year) Title. American Mineralogist, in press.
(DOI will not work until issue is live.) DOI: http://dx.doi.org/10.2138/am-2015-5149

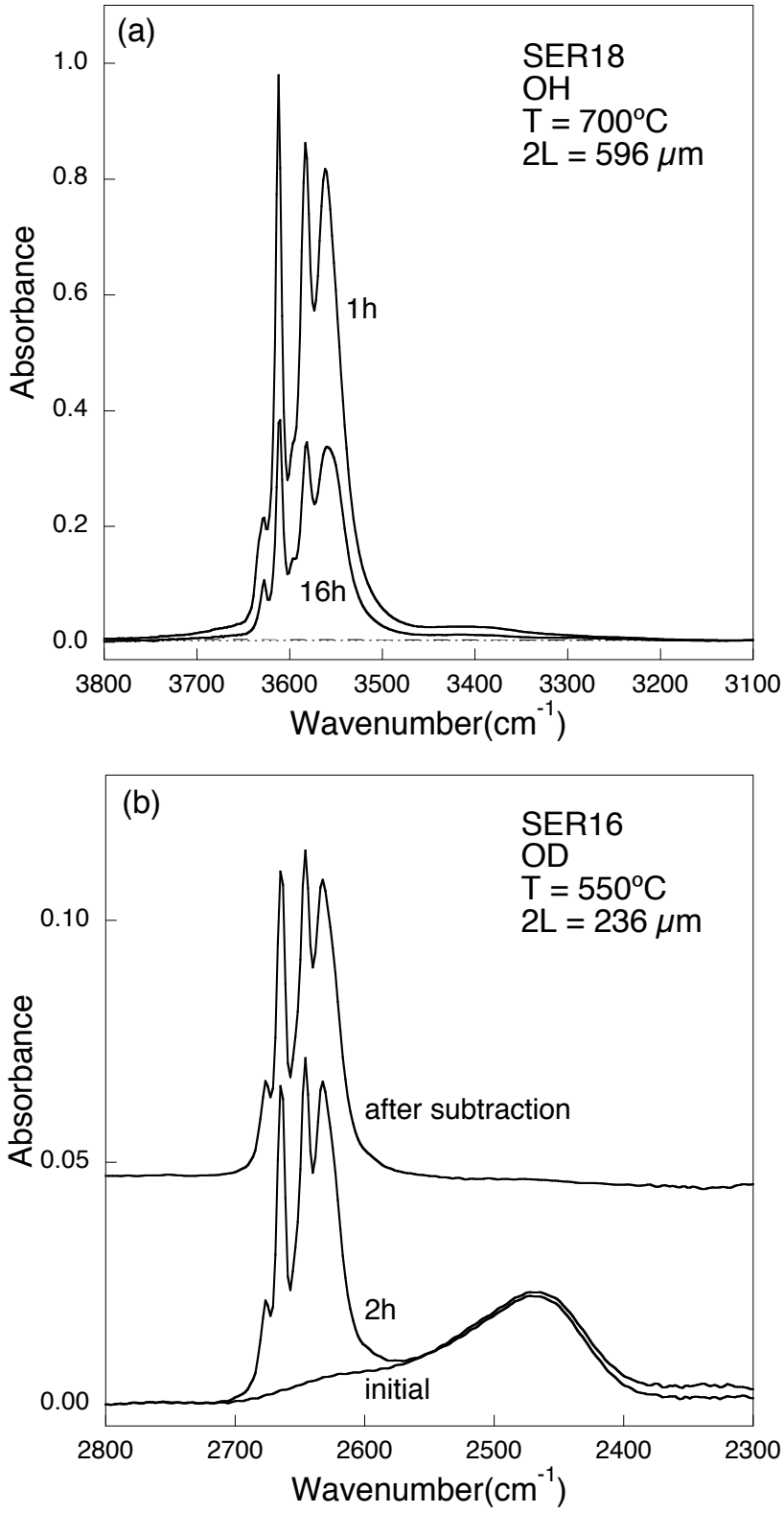

Fig. 1

This is a preprint, the final version is subject to change, of the American Mineralogist (MSA)
Cite as Authors (Year) Title. American Mineralogist, in press.
(DOI will not work until issue is live.) DOI: http://dx.doi.org/10.2138/am-2015-5149

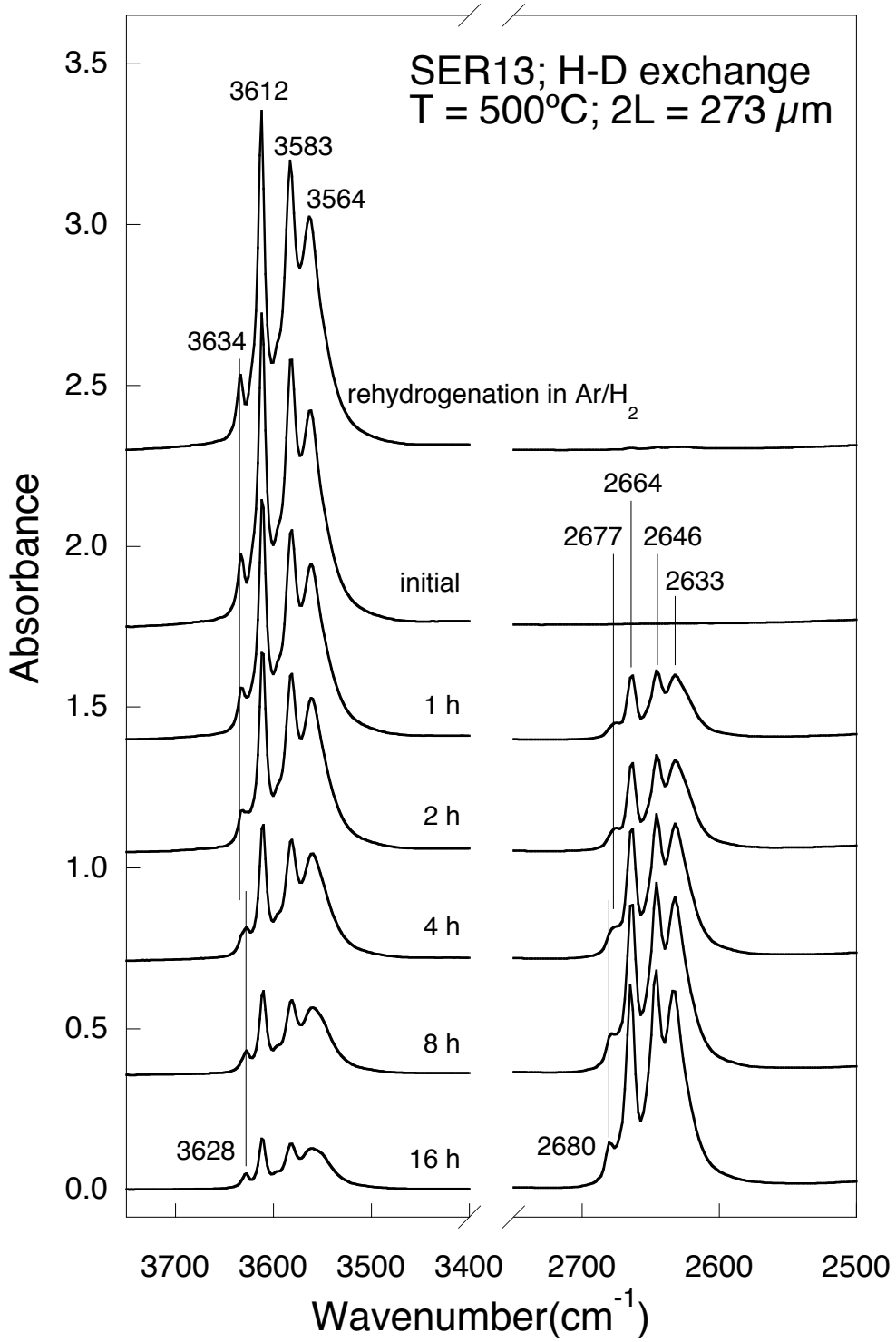

Fig. 2

This is a preprint, the final version is subject to change, of the American Mineralogist (MSA)
Cite as Authors (Year) Title. American Mineralogist, in press.
(DOI will not work until issue is live.) DOI: http://dx.doi.org/10.2138/am-2015-5149

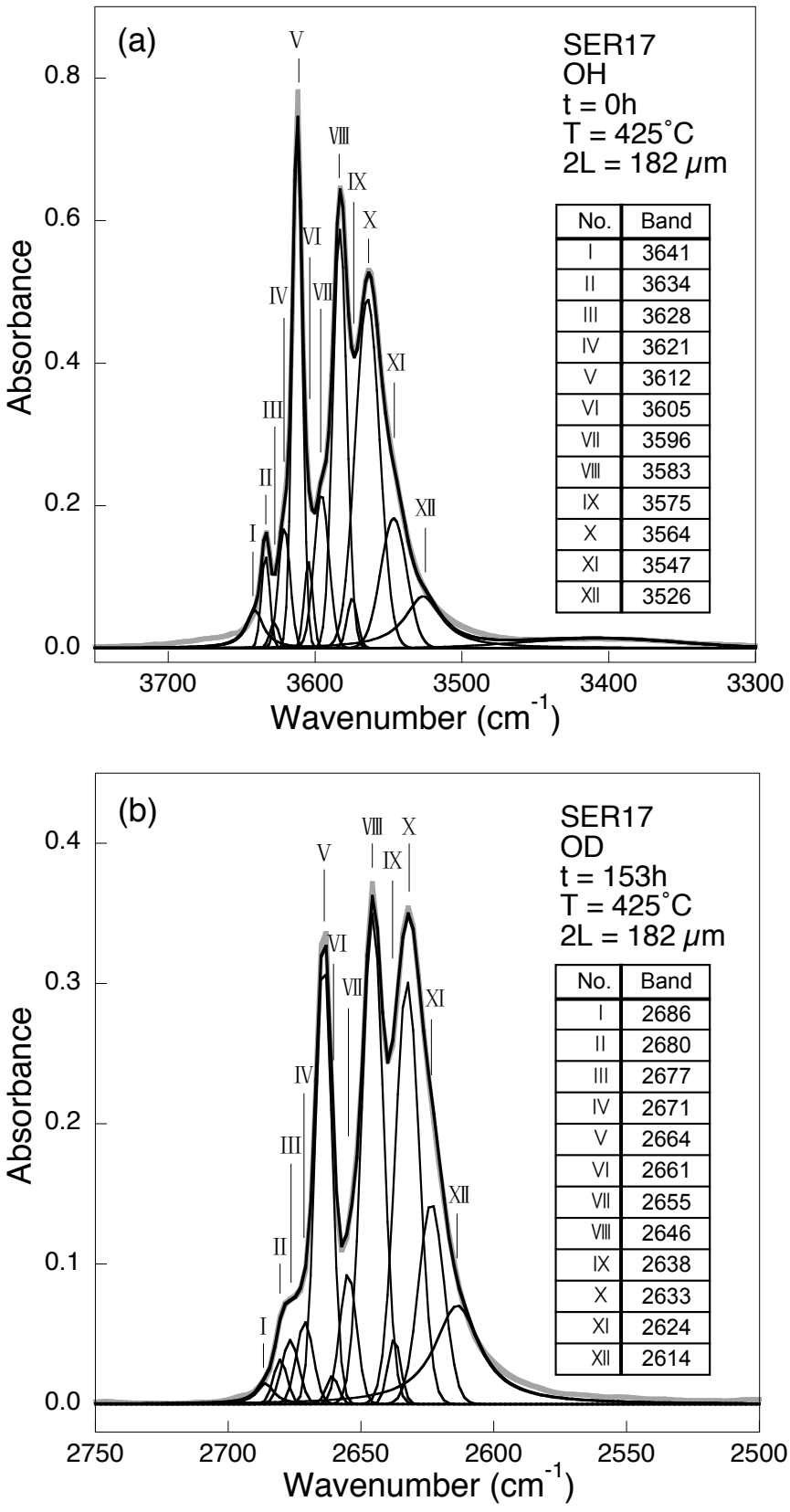

Fig. 3

This is a preprint, the final version is subject to change, of the American Mineralogist (MSA)
Cite as Authors (Year) Title. American Mineralogist, in press.
(DOI will not work until issue is live.) DOI: http://dx.doi.org/10.2138/am-2015-5149

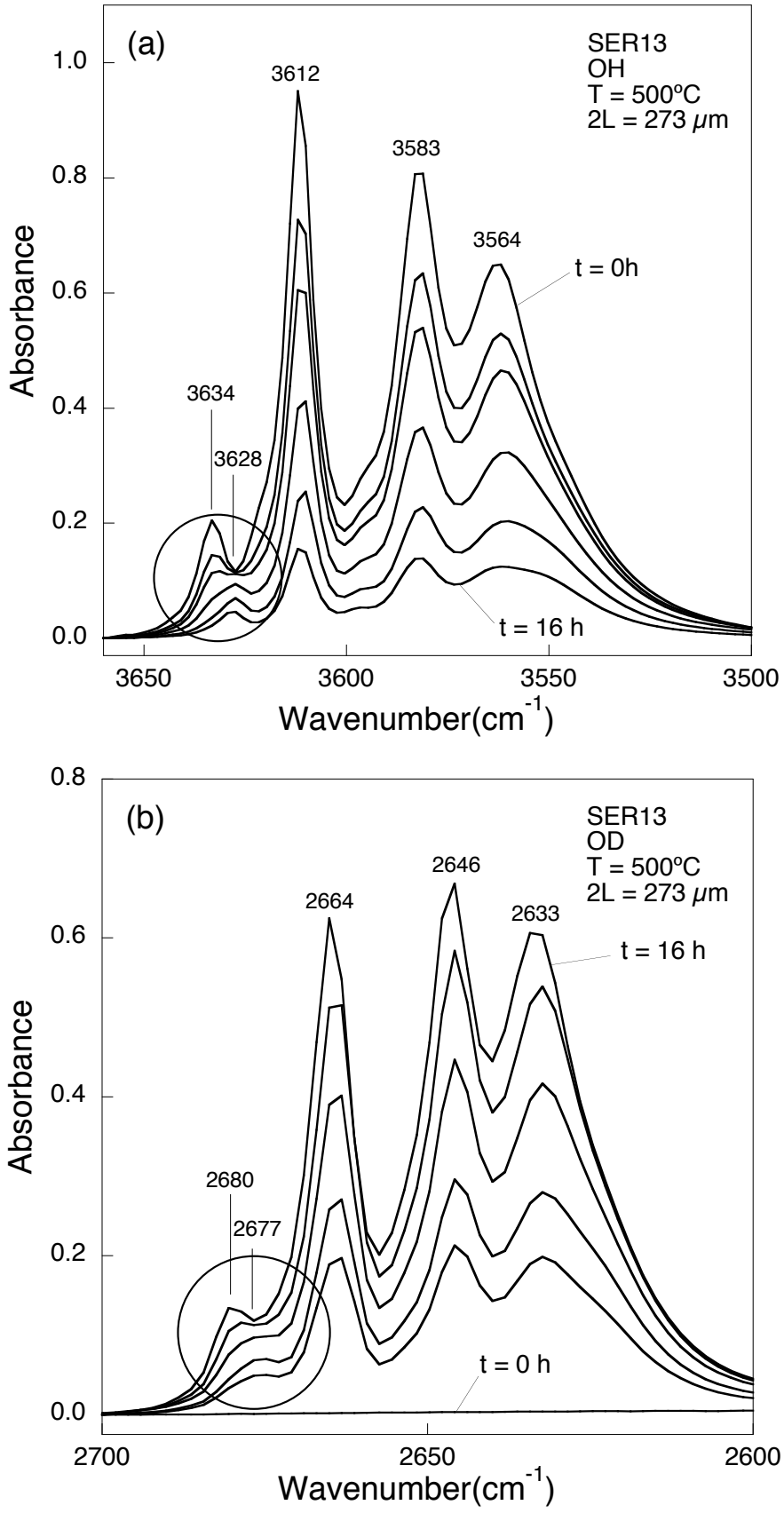

Fig. 4

This is a preprint, the final version is subject to change, of the American Mineralogist (MSA)
Cite as Authors (Year) Title. American Mineralogist, in press.
(DOI will not work until issue is live.) DOI: http://dx.doi.org/10.2138/am-2015-5149

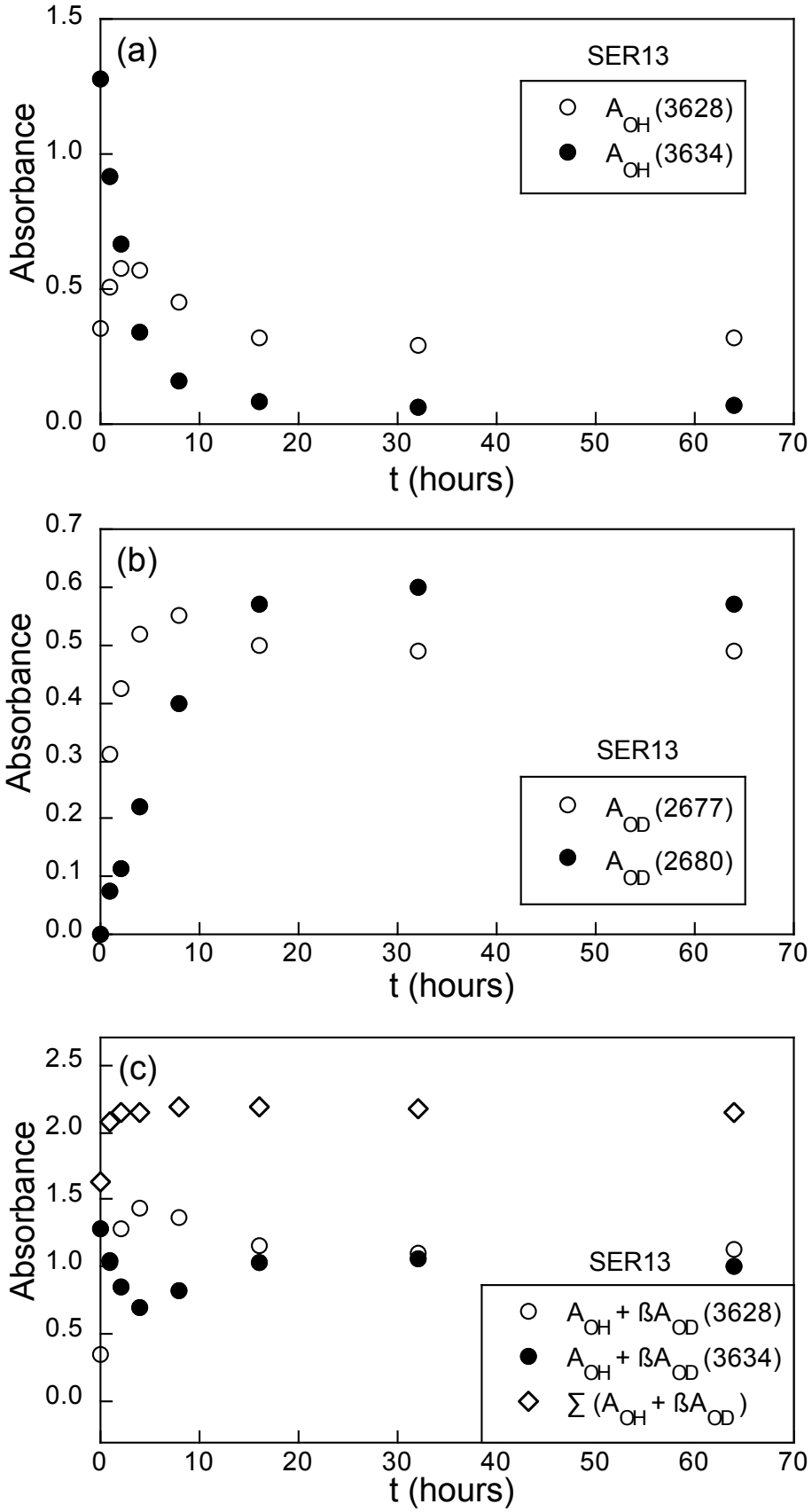

Fig. 5

This is a preprint, the final version is subject to change, of the American Mineralogist (MSA)
Cite as Authors (Year) Title. American Mineralogist, in press.
(DOI will not work until issue is live.) DOI: http://dx.doi.org/10.2138/am-2015-5149

Kinetics of deuteration in andradite

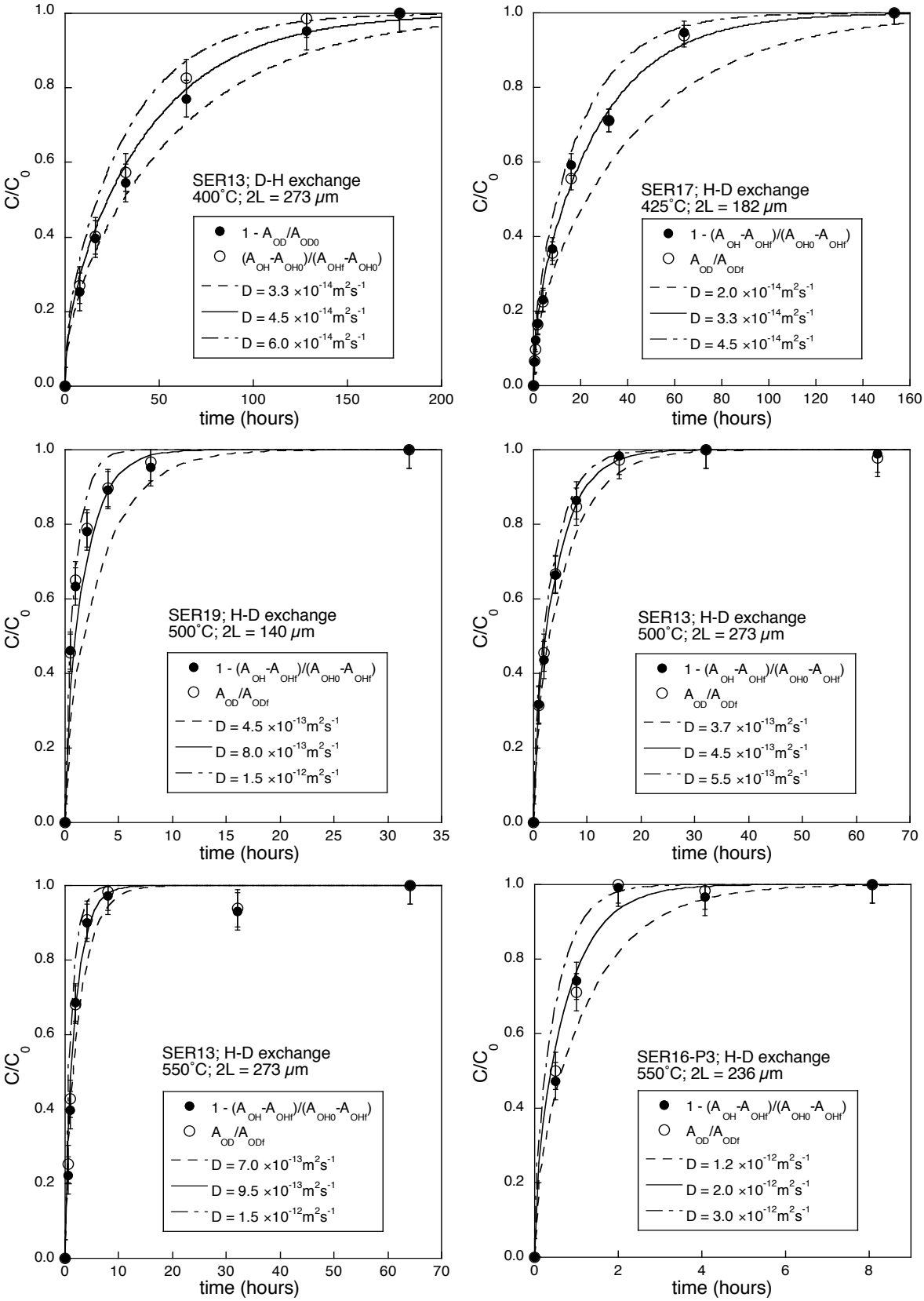

This is a preprint, the final version is subject to change, of the American Mineralogist (MSA)
Cite as Authors (Year) Title. American Mineralogist, in press.
(DOI will not work until issue is live.) DOI: http://dx.doi.org/10.2138/am-2015-5149

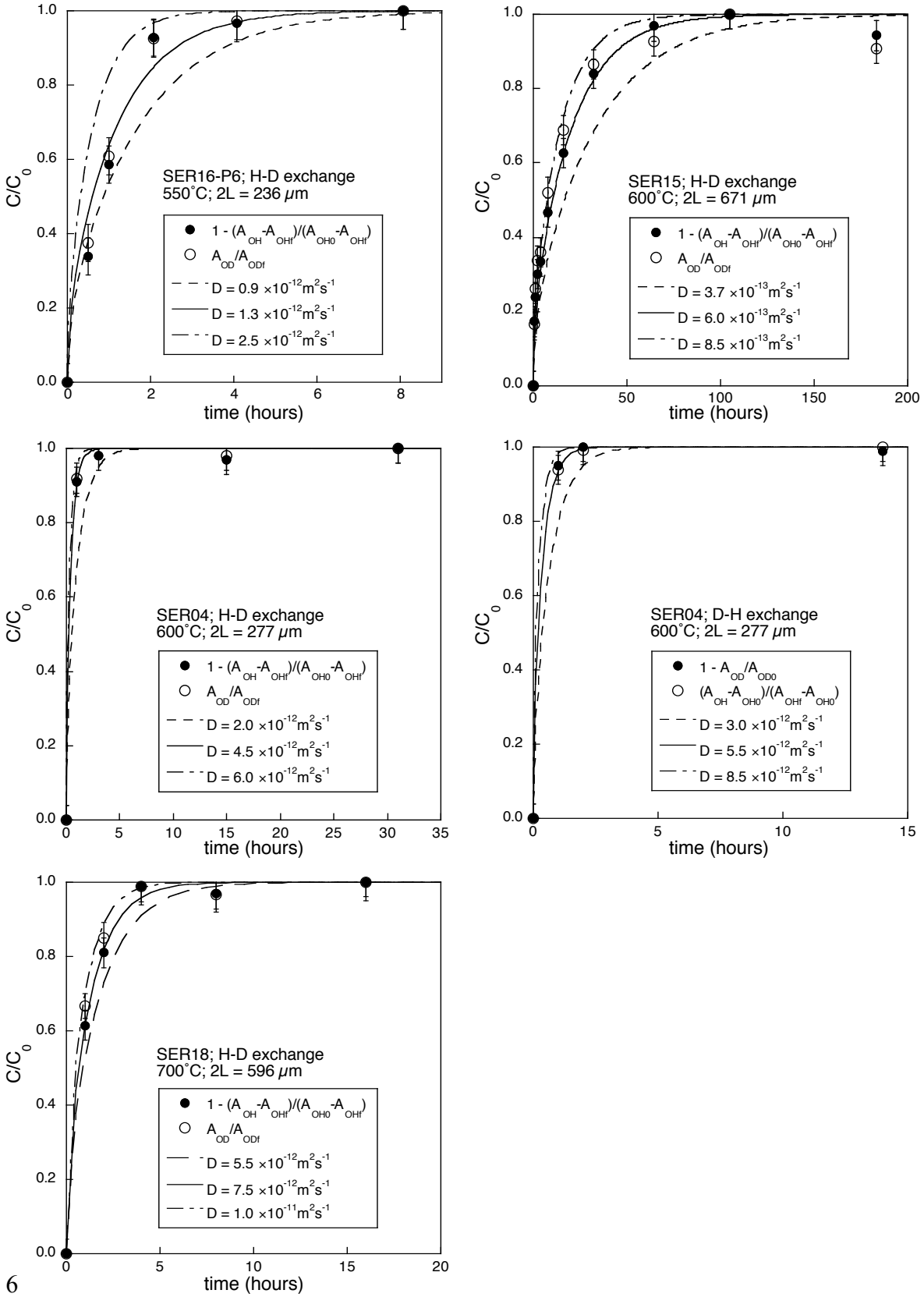

Fig. 6

This is a preprint, the final version is subject to change, of the American Mineralogist (MSA)
Cite as Authors (Year) Title. American Mineralogist, in press.
(DOI will not work until issue is live.) DOI: http://dx.doi.org/10.2138/am-2015-5149

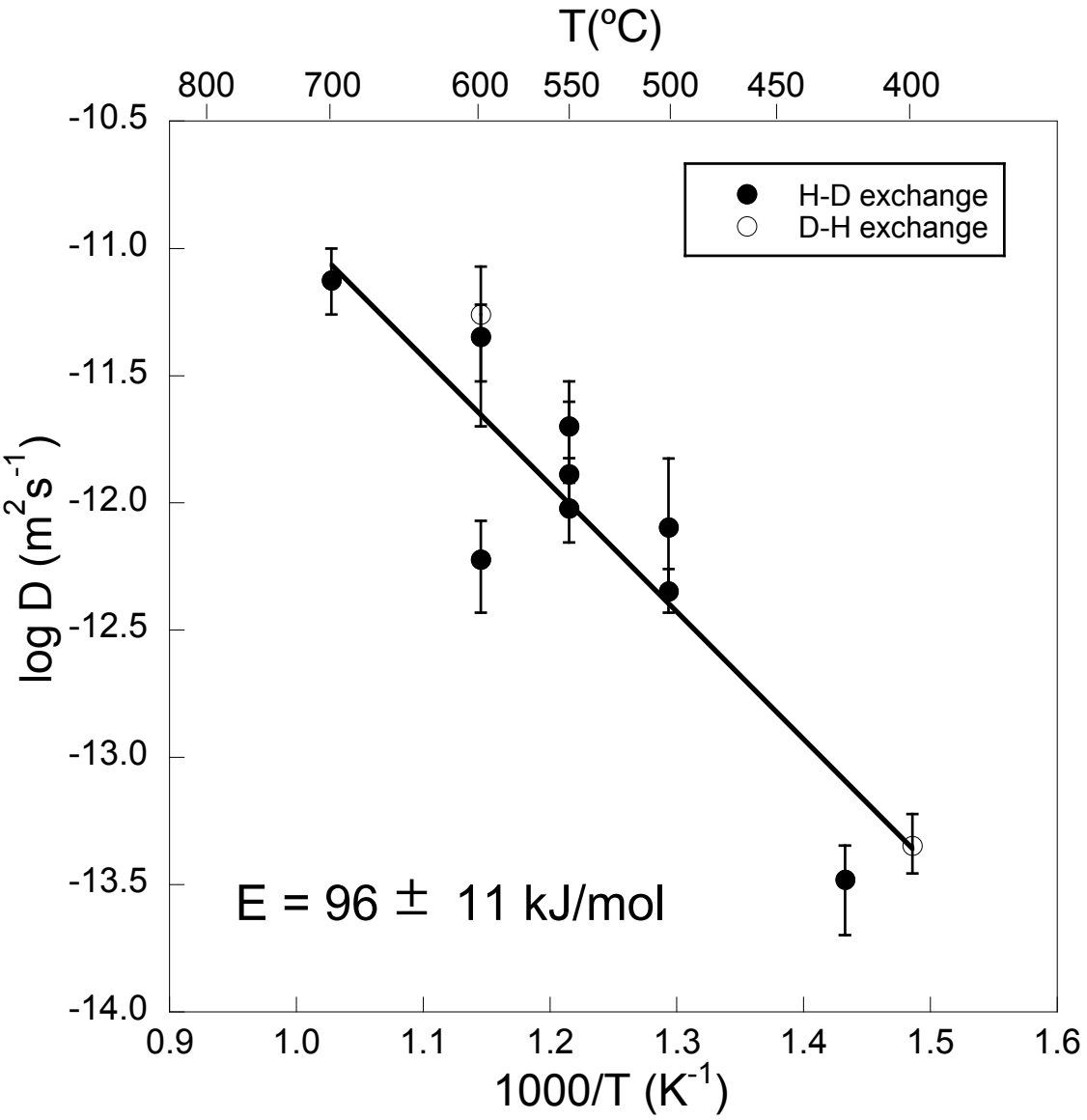

Fig. 7

This is a preprint, the final version is subject to change, of the American Mineralogist (MSA)
Cite as Authors (Year) Title. American Mineralogist, in press.
(DOI will not work until issue is live.) DOI: http://dx.doi.org/10.2138/am-2015-5149

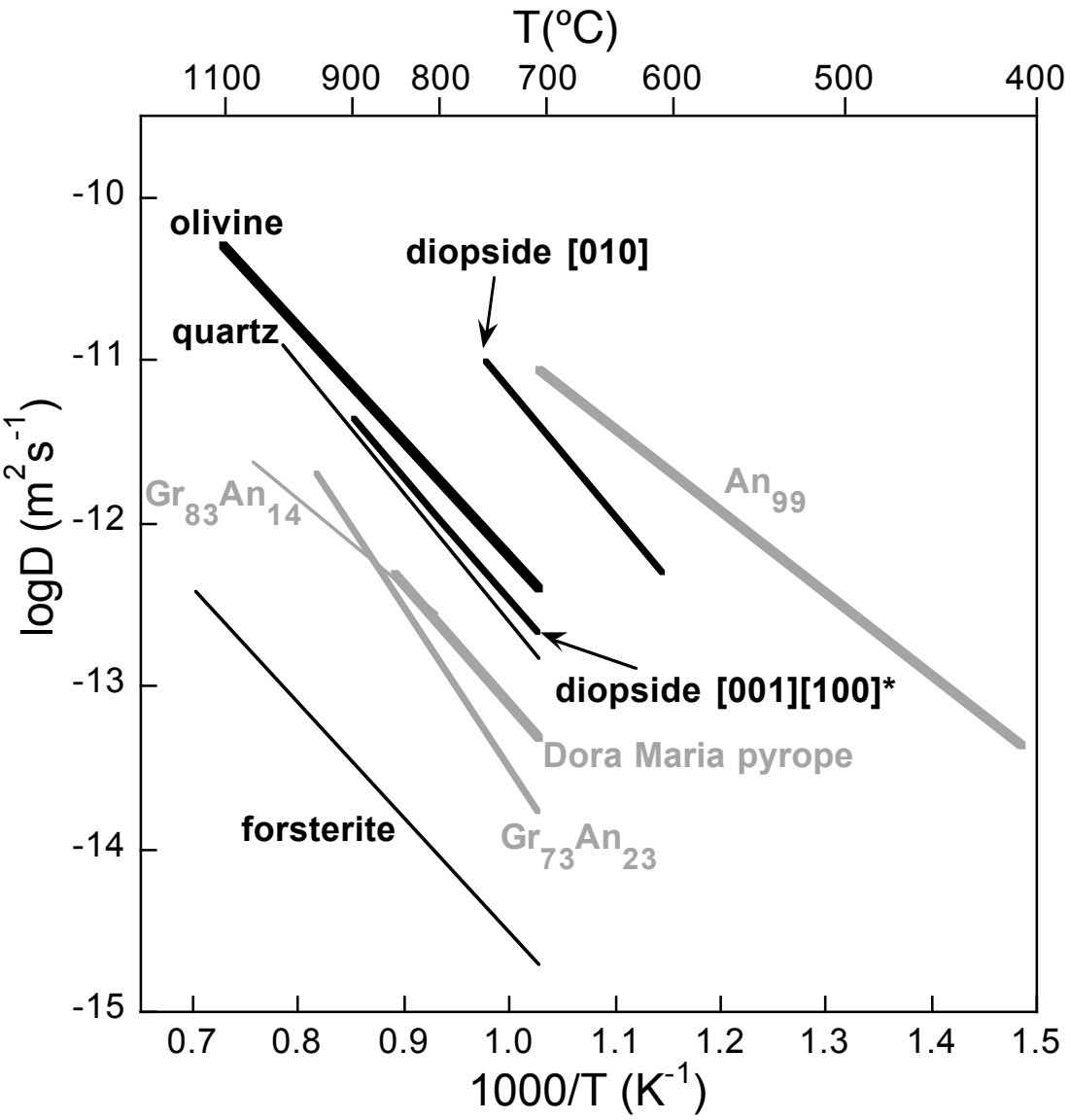

Fig. 8

This is a preprint, the final version is subject to change, of the American Mineralogist (MSA)
Cite as Authors (Year) Title. American Mineralogist, in press.
(DOI will not work until issue is live.) DOI: http://dx.doi.org/10.2138/am-2015-5149

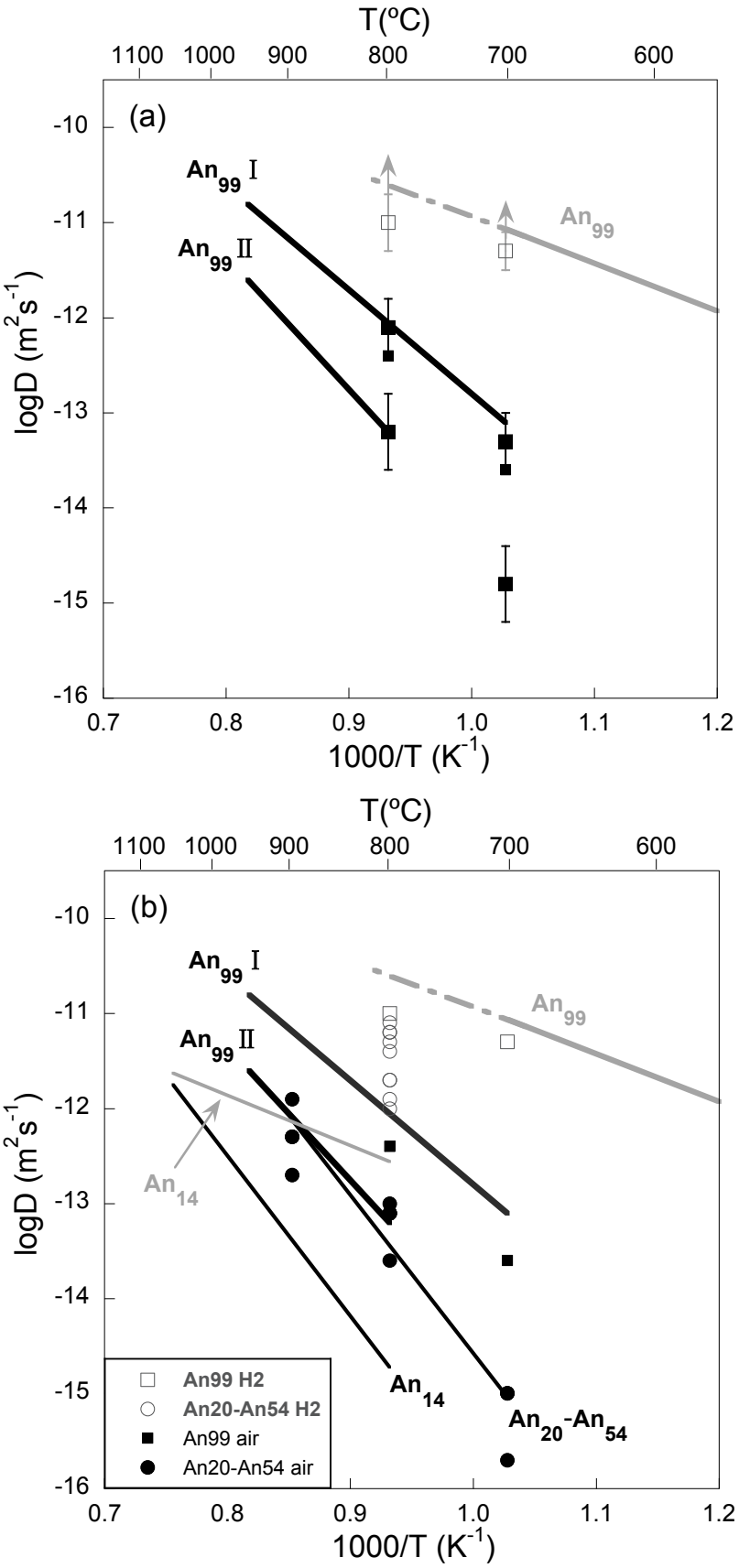

Fig. 9